

Phase-selective conductivity enhancement and cooperativity length in PLLA/TPU nanocomposite blends with carboxylated carbon nanotubes

Sofia Valenti^{a,b,1}, Omid Yousefzade^{a,c,1}, Jordi Puiggali^{a,d,**}, Roberto Macovez^{b,*}

^a Synthetic Polymers: Structure and Properties. Biodegradable Polymers Group, Chemical Engineering Department, Universitat Politècnica de Catalunya, EEBE, Av. Eduard Maristany 10-14, 08019 Barcelona, Catalonia, Spain

^b Grup de Caracterització de Materials, Departament de Física and Barcelona Research Center in Multiscale Science and Engineering, Universitat Politècnica de Catalunya, EEBE, Av. Eduard Maristany 10-14, 08019, Barcelona, Catalonia, Spain

^c Department of Polymer Engineering and Color Technology, Amirkabir University of Technology, 350, Hafez Ave, Tehran, Iran

^d Institute for Bioengineering of Catalonia (IBEC), The Barcelona Institute of Science and Technology, Baldiri Reixac 10-12, 08028, Barcelona, Spain

ARTICLE INFO

Keywords:

Nanofiller
Glass transition
Cooperatively rearranging region
Conductivity enhancement
Maxwell-Wagner-Sillars relaxation
Dielectric spectroscopy

ABSTRACT

Transmission electron microscopy, temperature-modulated differential scanning calorimetry, and broadband dielectric spectroscopy were employed to characterize ternary nanocomposites consisting of carboxylated carbon nanotubes (CNT) dispersed in a blend of two immiscible polymers, poly(L,lactide) (PLLA) and thermoplastic polyurethane (TPU). The nanocomposite blends were obtained by melt-compounding of PLLA and TPU in the presence of 0.2 wt-% CNT, either in the presence or absence of a Joncryl® ADR chain extender for PLLA, leading to reactive and non-reactive melt mixed samples. In both cases, the binary PLLA/TPU blend is characterized by phase separation into submicron TPU droplets dispersed in the PLLA matrix, and displays two separate glass transition temperatures. The carbon nanotubes are present either inside the TPU phase (samples obtained without chain extender), or at their boundaries (reactive-melt mixed samples). The effect of the sub-micron confinement of the TPU component is to decrease the cooperativity length of the primary segmental relaxation of this polymer, which is accentuated by the presence of the CNT fillers. Depending on the type of sample, five or six distinct relaxations are observed by means of dielectric spectroscopy, which we are able to assign to different dielectric phenomena. Our dielectric data show that the CNT fillers do not contribute directly to the long-range charge transport in the nanocomposite blends, consistent with the nanocomposites morphology, but rather result in a shift of the Maxwell-Wagner-Sillars space-charge frequency associated with charge accumulation at the PLLA/TPU boundary. Such shift testifies to a selective conductivity enhancement of the TPU phase due to the filler.

1. Introduction

Two main physical strategies are available to modify the properties of polymeric materials: on one hand, polymer blending; on the other, nanocomposite formation with suitable fillers. Most polymers are immiscible with one another; hence, their blends are not formed spontaneously and the final local morphology of the materials (phases formed, domain size, etc.) is nontrivial and depends in general on the preparation process. In a similar fashion, most (organic) synthetic

polymers do not display particular affinity for all (especially inorganic) fillers; the mutual affinity may in this case be improved by chemical functionalization of the filler to ensure the formation of nanocomposites with more homogeneous dispersion properties [1,2].

Polymer blends and (nano)composites represent the majority of all commercialized polymers, with polymer blending alone representing 36% of all polymer consumption [3]. The ever-increasing demand for plastic materials drives research to discover better, more economic alternatives with superior combinations of properties as a replacement for

* Corresponding author. Grup de Caracterització de Materials, Departament de Física and Barcelona Research Center in Multiscale Science and Engineering, Universitat Politècnica de Catalunya, EEBE, Av. Eduard Maristany 10-14, 08019, Barcelona, Catalonia, Spain.

** Corresponding author. Synthetic polymers: Structure and properties. Biodegradable polymers Group, Chemical Engineering Department, Universitat Politècnica de Catalunya, EEBE, Av. Eduard Maristany 10-14, 08019, Barcelona, Catalonia, Spain.

E-mail addresses: jordi.puiggali@upc.edu (J. Puiggali), roberto.macovez@upc.edu (R. Macovez).

¹ These authors contributed equally to the paper.

the more traditional polymers. This has resulted in research on and implementation of multicomponent and multiphase materials (beyond binary or ternary blends) and of new processing methods (such as gas and multiple injection processes, melt-core technology, or microcellular foams). The general goals of both polymer blending and dispersion of nanofillers is the improvement of mechanical and rheological properties, or the enhancement of the material's electrical conductivity or resistance to environmental factors (heat, light irradiation, diffusion of gases, wetting with liquids) [4–9]. From a fundamental point of view, the blending of two immiscible polymers, the admixture of nanofillers to a single polymer, and even the synthesis of copolymers, all represent different strategies for obtaining nontrivial morphologies through (non-equilibrium) self-assembly, which can be exploited for the design of advanced nanostructured materials.

Poly(L-lactide) (PLLA) is a biodegradable polymer that can be derived from renewable bio-sources such as sugar and starch and which has received considerable interest in the past decades for both commodity and specialty applications, both as pure material [10,11] and as a component of nanocomposites [12,13]. Concerning blends, many researchers have focused on the improvement of mechanical properties and thermal stability of PLLA by blending it with other polymers [14]. A number of studies has shown that blending PLLA with a polyurethane thermoplastic (TPU) leads to enhanced toughness [15–19].

Most fundamental studies deal with the characterization of binary polymer blends or of binary systems made of a filler dispersed in a single polymer. In this contribution we explore some fundamental physical properties of a ternary nanocomposite system consisting of multi-wall carbon nanotubes (CNTs) dispersed in a blend of two different polymers (PLA and TPU). The samples are obtained by melt-compounding a PLLA-CNT nanocomposite with a PLLA/TPU blend either in the presence or absence of commercial multifunctional styrene-acrylic oligomers (BASF, Joncryl® ADR-4368) which were used as a PLLA chain-extender reactive agent. We study the morphology of the resulting nanocomposite blends and the effect of the CNTs filler on the cooperative and local relaxation dynamics, and on the size of the cooperative rearranging regions in both polymer components. Given that the presence of CNTs may enhance the electrical conductivity of the nanocomposites, we also study their impact both on the dc conductivity of the samples and on interfacial space-charge relaxations.

2. Experimental

Poly(L-lactide) (PLLA grade 4032D), containing 2% of D-lactide units, was purchased from Natureworks LLC, USA, while the thermoplastic polyurethane (TPU, grade RAVATHANE® R120A65) was supplied by Ravago Manufacturing Americas. Multi-wall CNTs with 9.5 nm average diameter, 1.5 μm average length, and specific surface area of ca. 250–300 $\text{m}^2 \text{g}^{-1}$ were provided by Nanocyl (Nanocyl7000 series, Belgium). To enhance the affinity of the carbon nanotubes for the polymer matrices and thus their homogeneous dispersion, carboxylated multi-walled carbon nanotubes CNTs were prepared via an acid oxidation process [20]. A PLLA/CNTs masterbatch with 5 wt-% of CNTs was then prepared by solution casting to improve the dispersion state.

To obtain blends and nanocomposites, pure PLLA and the PLLA/CNT dispersion were melt-compounded with the appropriate amounts of a PLLA/TPU blend with a TPU proportion of 20 wt-%. Commercial multifunctional styrene-acrylic oligomers (BASF, Joncryl® ADR-4368) were used as a PLLA chain-extender reactive agent. The mixing in the molten state was carried out at 190 °C either in the presence or absence of the chain extender, leading to reactive and non-reactive melt mixing, respectively. A laboratory internal mixer (Brabender mixer, PL2200) operating at a rotor speed of 60 rpm was employed for this purpose. The amount of the chain modifier for reactive melt mixing was set to 0.5 wt-%. Chain-extension reactions were considered completed when a plateau in torque curves was achieved. All samples were rapidly cooled in cold water to prevent crystallization and thereby obtain completely

amorphous samples. The studied samples are named by the abbreviation PT/CNTx/Y. The number after CNT shows its weight fraction in the nanocomposite. The upper case letter at the end of the code indicates reactive (R) or non-reactive (N) melt mixing, e.g. PT/CNT0.2/R corresponds to the nanocomposite containing 0.2 wt-% of MWCNTs prepared by reactive melt mixing.

Transmission electron microscopy (TEM, Philips TECNAI 10 operating at 80 kV) was employed to evaluate the selective localization of MWCNTs in the as-prepared nanocomposites. For these experiments, TPU was selectively stained using OsO_4 vapors to enhance the contrast with the PLLA matrix.

2.1. Characterization by broadband dielectric spectroscopy

Isothermal dielectric spectra were acquired with an Alpha Analyzer by Novocontrol Technologies GmbH & Co., placing a nanocomposite or blend membrane with a thickness of approximately 0.2 mm between two stainless steels electrodes of 21 mm diameter. Dielectric spectroscopy yields the complex relative permittivity of the sample, $\epsilon^*(f) = \epsilon'(f) - i\epsilon''(f)$, as a function of frequency f . The imaginary part $\epsilon''(f)$, called the loss spectrum, is related to the conductivity as $\sigma'(f) = 2\pi f \epsilon_0 \epsilon''(f)$. The thickness of the membrane and of the capacitor were measured with a caliper and used to calibrate the permittivity and conductivity scales. Temperature control of the capacitor was achieved with a Novocontrol Quatro nitrogen-gas flow cryostat with a temperature stability better than 0.3 K. Isothermal spectra were acquired in the frequency range between 10^{-1} Hz and 10^6 Hz, varying the temperature in a stepwise manner between 123 and 423 K (in the case of the bulk TPU sample, the temperature range was extended to 473 K), every 2 or 5 K.

The loss spectra $\epsilon''(f)$ were fitted as the sum of separate model functions, one for each dipolar relaxation process, and a dc conductivity background, which was experimentally visible only above the glass transition temperature of the PLLA component. Each relaxation was modeled as the imaginary part of a phenomenological Havriliak-Negami function, given by Refs. [21,22]:

$$\epsilon_{HN}''(f) = \frac{\Delta\epsilon}{(1 + (i2\pi f\tau_{HN})^c)^d} \quad (1)$$

Here, $\Delta\epsilon$ is the dielectric strength (intensity) of the relaxation process, the exponents c and d are shape parameters related to the tails of the loss peak in logarithmic representation, and τ_{HN} is a fitting parameter from which the relaxation time τ at which the loss is maximum can be obtained as:

$$\tau = \tau_{HN} \left(\sin \frac{c\pi}{2+2d} \right)^{-1/c} \left(\sin \frac{cd\pi}{2+2d} \right)^{1/c} \quad (2)$$

A special case of the Havriliak-Negami function is the Cole-Cole function [23,24], which corresponds to Eq. (1) with $d = 1$ (and $c \neq 1$). While the imaginary part of the Havriliak-Negami function has an asymmetric line shape, that of the Cole-Cole function is symmetric, and for this special case the parameter τ_{HN} coincides with the time τ at which the imaginary permittivity is maximum, as can be inferred from Eq. (2). While we always performed fits using the Havriliak-Negami function, for some of the relaxation features the fit automatically converged to the value $d = 1$, implying that the corresponding feature had a symmetric profile, better described by a Cole-Cole function.

2.2. Temperature-modulated DSC characterization

Temperature-modulated DSC thermograms were acquired with a TA Instrument DSC Q100 calorimeter. Experiments were performed in a nitrogen atmosphere with a flow rate of 50 mL/min. Samples consisting of blends with or without the CNT filler, and with a total mass of 4–5 mg, were loaded in aluminum pans. The modulated temperature program corresponded to a sinusoidal temperature profile in the range between

198 and 353 K with a heating rate of 2 K/min, amplitude of 0.32 K, and modulation period of 60 s.

3. Results and discussion

3.1. General morphology, calorimetric traces, and dielectric behavior of the samples

In a recent article [25] it has been shown that the morphology of the PLLA/TPU/CNT nanocomposite blends is nontrivial and depends on the mixing step at 190 °C. TEM imaging was employed to study the localization of CNTs. The TEM micrographs displayed in Fig. 1 demonstrate that the CNTs form a network structure in the nanocomposite material. The final morphology of the nanocomposite blends is strongly dependent on whether the samples are obtained by reactive or non-reactive mixing. In particular, for non-reactive melt-compounded samples, the filler is dispersed in the bulk TPU phase, while in the samples obtained from the reactive-melt, the CNTs lay at the interface between TPU and PLLA, creating a partial barrier between the two polymers. This difference in morphology induced by selective localization of nanoparticles has been also reported also in blends of other polymers [26–28]. Both results are intriguing, considering that the CNTs are initially dispersed in the PLLA phase, and show that carboxylated CNTs have more affinity for the more polar TPU polymer than for PLLA, unless the latter is modified with the chain extender.

Visual inspection of Fig. 1 shows that each TPU droplet contains only few CNTs. This is in line with a rough estimate based on the weight fraction of the filler: if all the CNTs are present in the TPU phase, then the weight fraction of the filler in TPU is $(0.002 \cdot 100)/20 = 1\%$. Assuming, following previous studies [29,30], that the average mass density of the functionalized CNTs is similar to that of graphite, hence roughly 1.75 times that of TPU in the melt (as per manufacturer specifications), this entails that the volume fraction of nanotubes in the TPU phase should be of the order of 0.6%, which is close to the reported percolation threshold for filler-induced electrical conductivity in TPU functionalized with carboxylated CNTs [31]. The typical volume occupied by a nanotube is, according to the manufacturer's specifications (see Section 2), of the order of $1.5 \cdot \pi \cdot (5 \cdot 10^{-3})^2 \mu\text{m}^3 = 1.2 \cdot 10^{-4} \mu\text{m}^3$. In a TPU droplet of 500 nm of diameter and thus a volume of $6.5 \cdot 10^{-2} \mu\text{m}^3$, the volume occupied by the nanotubes should be 0.6% of this, equivalent to roughly 4 CNTs per droplet.

Given these results, it is interesting to determine how the different morphology affects the temperature-dependent segmental motions and dielectric relaxation and conduction properties of the nanocomposite blends, and compare them with the blends without carbon nanotubes and with the pure polymers separately. We start by analyzing the relaxation dynamics of the binary PLLA/TPU blends, which display five different relaxations, and then discuss the effect of the CNTs on the relaxation dynamics of the (ternary) nanocomposite blends.

Fig. 2(a) displays the loss factor ($\tan \delta = \epsilon''(f)/\epsilon'(f)$) at 1 Hz as a function of temperature, both for the blends and the nanocomposites. Four different relaxation features are observed, of which two relatively sharp ones at ca. 233 and 330 K. As visible in the DSC thermograms of the samples, displayed in Fig. 2(b), the latter temperature corresponds to the glass transition temperature (T_g) of pure PLLA [32], while the former matches the T_g of bulk TPU (also shown in Fig. 2(b)). The corresponding dielectric features can therefore be assigned to the cooperative segmental relaxations respectively of the PLLA and TPU components of the blends, whose kinetic arrest marks the glass transition temperature of each phase. The other two loss features visible in Fig. 2(a) correspond instead to the secondary (β) relaxations of both polymers (feature centered at ca. 173 K) and to an interfacial Maxwell-Wagner-Sillars space-charge relaxation (at ca. 290 K), both to be discussed further on.

In order to better identify all spectral features, we acquired isothermal complex permittivity spectra at various temperatures ranging from 123 to 423 K. In Fig. 3 we plot the isothermal dielectric loss spectra $\epsilon''(f)$ for all four samples studied, at few selected temperatures.

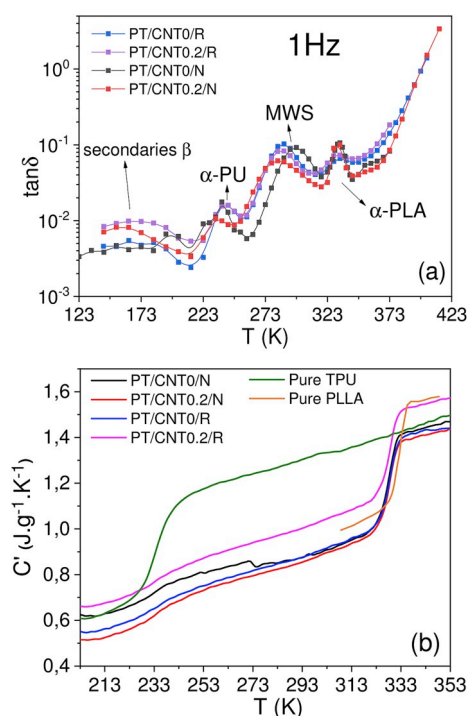


Fig. 2. Temperature-dependent loss factor (a) and DSC thermograms (b) of all four types of samples studied. In (b), the thermograms of pure bulk TPU and PLLA are also shown for comparison.

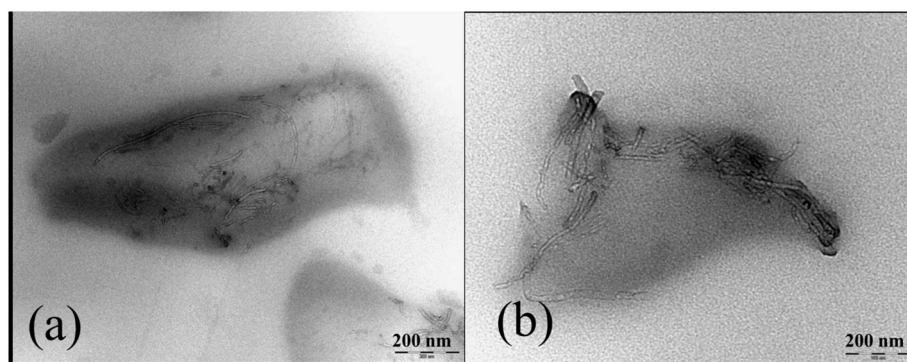


Fig. 1. TEM images of different nanocomposite blends with 0.2% CNTs in weight, obtained either by nonreactive (a) or reactive melt-compounding (b). Notice the different localization of the CNTs, either in the bulk TPU phase or at the interface between TPU and PLLA.

The loss spectra display several features which shift to higher frequency with increasing acquisition temperature.

As mentioned in Section 2, the raw imaginary permittivity $\epsilon''(f)$ spectra were fitted as the sum of distinct spectral components to extract quantitative information on the relaxation time and dielectric strength of each loss feature. The fit procedure was not always trivial, as two relaxations overlapped one another in some of the spectra; we were nonetheless able to separate both contribution relying on the very different temperature dependence of both (see also below). The relaxation times of all loss processes present in the samples obtained by non-reactive melt mixing (Fig. 3(a and b)) are shown as Arrhenius plots in Fig. 4(a); those of the reactive-melt mixing samples (Fig. 3(c and d)) are reported in Fig. 4(b). For comparison purposes, the relaxation times of the primary and secondary relaxation dynamics of the pristine PLLA matrix without chain extender (filled yellow triangles) [32,33] and of pure TPU (filled green squares) that we acquired with our set-up are also shown in both panels of Fig. 4. The data for TPU are in agreement with previous studies [34].

3.2. Glass transition and cooperativity length in both polymer phases

The segmental relaxations of both pristine bulk PLLA and bulk TPU display a non-simply activated behavior, typical of primary structural relaxations. Among the relaxations of the blends and nanocomposites obtained by non-reactive mixing, two of them showed characteristic

times with roughly the same values and similar temperature dependence of the primary segmental relaxations of the pure polymers. In the loss spectra, all primary segmental relaxations (of pure PLLA, pure TPU, and of the PLLA and TPU components in the blends) were fitted with a Havriliak-Negami function (Eq. (1)). This is a common procedure for primary structural relaxations, given the asymmetry of their loss feature in most glass formers. The typical values of the Havriliak-Negami exponents were in the ranges $c = 0.35$ – 0.7 , and $d = 0.5$ – 0.7 , for PLLA, and $c = 0.2$ – 0.4 , and $d = 0.5$ – 0.7 , for TPU.

For both segmental relaxations, labeled as α_{PLLA} and α_{TPU} in Figs. 3 and 4, a kinetic glass transition temperature can be defined as the temperature at which the relaxation time reaches a value of 100 s (i.e. $\log_{10}(\tau) = 2$, represented by the dashed horizontal line in Fig. 4). In order to obtain a more accurate estimation of the kinetic glass transition temperature of both components, the temperature dependent relaxation times of the primary relaxations were fitted with a Vogel-Fulcher-Tammann equation (not shown), whose analytical expression is [35]:

$$\tau_{\max} = \tau_0 \exp[D T_{\text{VF}} / (T - T_{\text{VF}})]. \quad (3)$$

The value of the phenomenological parameters intervening in this expression, namely the prefactor τ_0 , the fragility parameter D , and the Vogel-Fulcher temperature T_{VF} , are listed in Table 1 for each segmental relaxation of the four blend samples, together with the kinetic glass transition obtained by extrapolating the value of the Vogel-Fulcher-Tammann equation at $\tau = 100$ s. The kinetic T_g of both primary

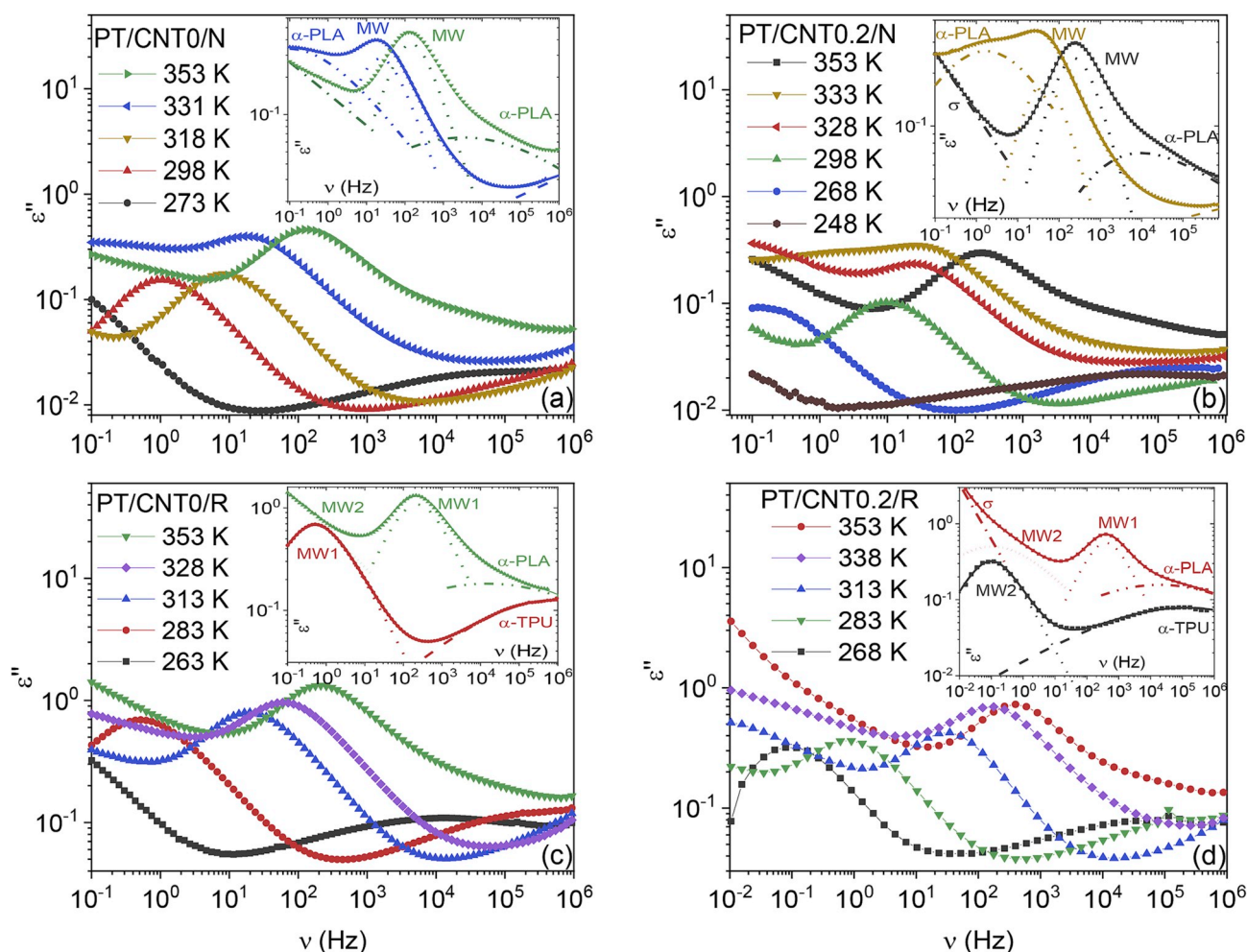


Fig. 3. Loss spectra of the blends obtained via non-reactive (a and b) and reactive mixing (c and d), both without (a and c) and with (b and d) CNT nanofillers, at the indicated temperatures. Insets: fit and fit components of the loss spectra at two selected temperatures for each sample, displayed together with the corresponding raw spectra to visualize the fit quality.

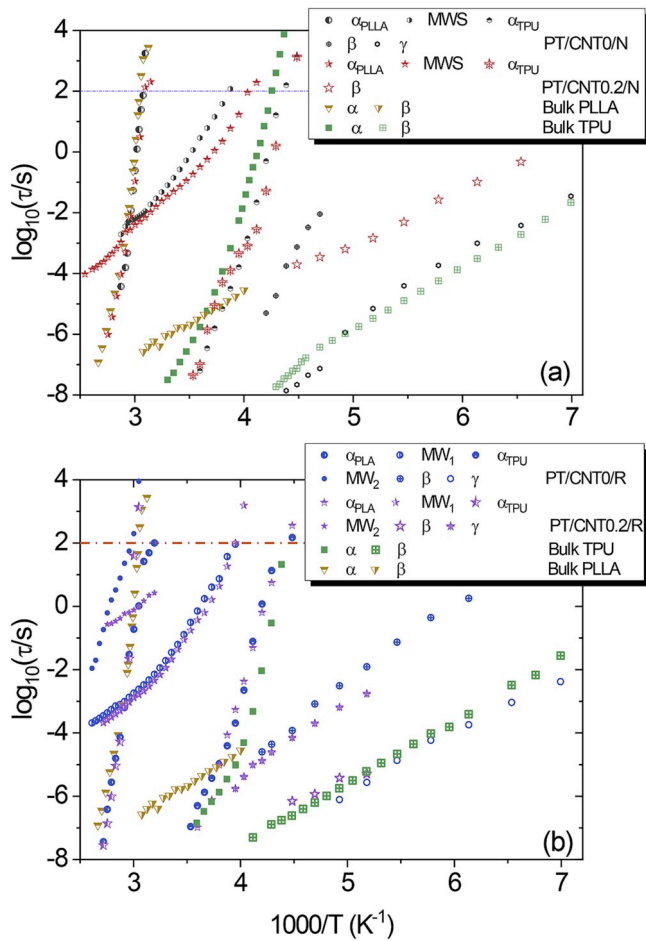


Fig. 4. Arrhenius plot of the relaxation time of the dielectric losses observed in the blend and nanocomposites obtained by non-reactive melt mixing (a) and by reactive melt mixing (b). For comparison, we report also the data for bulk PLLA (yellow triangles) and TPU (green squares). Filled symbols represent primary (α) relaxations, empty symbols and crossed symbols secondary (β , γ) relaxations, and half-filled symbols Maxwell-Wagner-Sillars space-charge relaxations. The horizontal dash-dotted line marks the relaxation time conventionally taken to correspond to the kinetic glass transition ($\log_{10}(\tau) = 2$). (For interpretation of the references to colour in this figure legend, the reader is referred to the Web version of this article.)

relaxations is roughly equal to the calorimetric T_g 's observed in Fig. 2 (b), as expected; however, the uncertainty associated with the determination of the kinetic T_g is much larger than that of a more direct method such as DSC.

The α_{PLLA} relaxation times of the blends in Fig. 4(a and b) are very close to those of the primary relaxation of pristine bulk PLLA (without chain extender). The kinetic T_g of bulk PLLA is slightly higher (by ca 4 K) than that of all four blend/nanocomposite samples. A possible rationalization of this effect of the PLLA phase is provided below. At the same

time, the relaxation time of the segmental relaxation of the TPU component in the blends is about one order of magnitude smaller than the bulk TPU data. This shift in segmental relaxation time entails a lower glass transition temperature of the TPU component. Since the polymers are immiscible, the observed changes cannot be due to any binary interaction. Moreover, comparison of the samples with and without CNT fillers shows that the cooperative segmental relaxation of the polymer is not strongly altered by the presence of the filler, in agreement also with what we observed in the PLLA-CNT nanocomposite [2]: there is only a small difference in relaxation time between the two types of samples studied, which exhibit instead a quite different distribution of the CNTs. We conclude that the most likely origin for the shift of the primary relaxation time of the either segmental relaxation (and the resulting shift in the kinetic T_g) with respect to the bulk polymers, is determined by interfacial effects.

Having identified two separate glass transition temperatures and segmental dynamics in the blends, we analyze the cooperativity length ξ_a (the size of the cooperatively rearranging regions at the glass transition) [36] in both polymer phases. According to the method developed by Donth [37–39], the volume of a cooperatively rearranging region $V_a = (\xi_a)^3$ can be estimated from the temperature fluctuations in the amorphous phase, as determined by complex heat capacity methods such as temperature-modulated DSC. In detail, the cooperativity length ξ_a for each polymer phase is given by Ref. [37]:

$$V_a = (\xi_a)^3 = k_B \left(\frac{T_g}{\delta T} \right)^2 \frac{\Delta C_p^{-1}}{\rho}, \quad (4)$$

where ρ is the mass density at T_g , ΔC_p^{-1} is the difference between the inverse of the isobaric heat capacity at T_g in the viscoelastic and the glass phase, and δT is the mean temperature fluctuation in a cooperatively rearranging region. The latter is usually assumed to be equal to the standard deviation of the dissipation peak $C''(T)$ in DSC.

Fig. 5 shows the imaginary parts of the specific heat curves of all samples, as obtained in our temperature-modulated DSC experiments. The fit values of T_g and δT determined assuming a Gaussian line shape are reported in Table 2. It is seen that blending with TPU decreases the glass transition of PLLA domains by 4 K, an effect which is independent of the presence of chain extender or of the addition of CNT and which is in agreement with our dielectric spectroscopy data. The lack of an effect of the nanofillers on the T_g of the PLLA component is to be expected due to their localization in the TPU phase.

The cooperative length in the PLLA matrix and the TPU phase (of the order of 2 or 3 nm) is much smaller than the linear size of TPU droplets in the blends (i.e., 500–900 nm). It may be observed that the cooperativity length of the TPU component is significantly reduced with respect to the bulk polymer. This is possibly a consequence of the submicron confinement in the relatively rigid PLLA matrix: the submicron TPU droplets have a relatively large interface area with PLLA; the latter is, at the temperatures where the segmental relaxation of the TPU phase becomes activated, deep in the glass phase. The interface of TPU with PLLA might result in a relatively rigid amorphous TPU surface layer, in a similar way as the interface of an amorphous domain with a crystalline domain in semicrystalline polymers leads to the appearance of a rigid

Table 1

Vogel-Fulcher-Tammann parameters and kinetic T_g for both PLLA and TPU components in the studied hybrid samples.

Sample	TPU				PLLA			
	T_g [K]	T_{VF} [K]	D	$\log_{10}(\tau_0/s)$	T_g [K]	T_{VF} [K]	D	$\log_{10}(\tau_0/s)$
Pure PLLA	—	—	—	—	328 ± 1	289 ± 1	3.7 ± 0.2	−12.7 ± 0.3
Pure TPU	235 ± 2	174 ± 2	6.5 ± 0.4	−16.5 ± 0.4	—	—	—	—
PT/CNT0/N	231 ± 3	175 ± 3	6.1 ± 0.4	−17.2 ± 0.5	327 ± 2	287 ± 2	2.4 ± 0.8	−15.4 ± 0.6
PT/CNT0.2/N	227 ± 3	174 ± 2	5.4 ± 0.2	−16 ± 1	323 ± 3	277 ± 3	2.9 ± 0.3	−15.4 ± 0.6
PT/CNT0/R	234 ± 8	187 ± 8	4 ± 1	−14 ± 1	323 ± 4	275 ± 4	3.2 ± 0.3	−16 ± 1
PT/CNT0.2/R	231 ± 6	178 ± 6	5.7 ± 0.7	−17.3 ± 0.4	331 ± 7	295 ± 7	2.2 ± 0.8	−16 ± 2

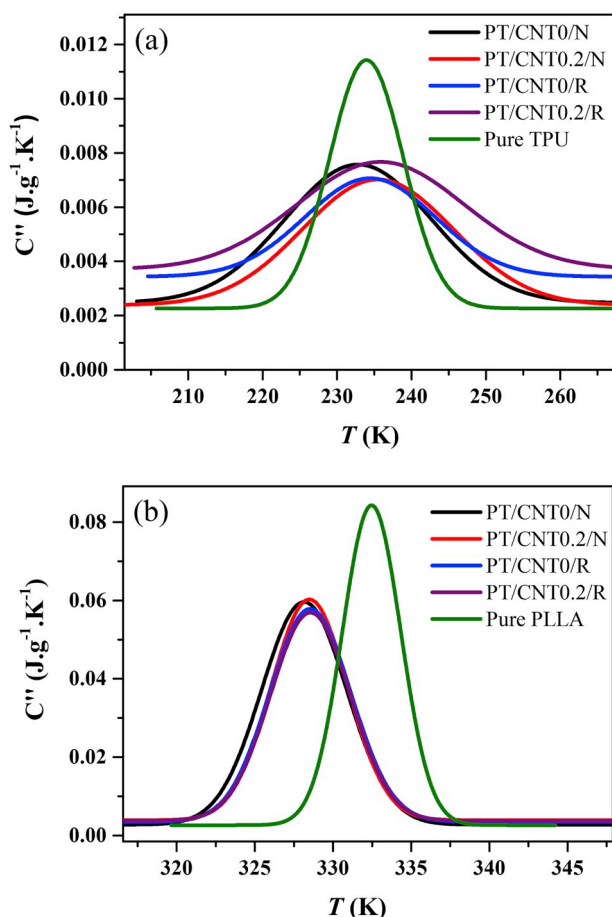


Fig. 5. Imaginary part of the calorimetric response across the glass transition of (a) TPU (233 K) and (b) PLLA (329 K) components of the nanocomposite blends, for all four types of samples studied. In both panels the pure bulk polymer is also shown for comparison.

amorphous polymer fraction in its proximity. This rigidity would then effectively limit the size of cooperatively rearranging region size near the TPU-PLA boundary.

The cooperativity length of the TPU phase is further reduced by the presence of the CNT fillers, an effect that may be expected since the CNTs are located inside the intrusions or at their boundaries and therefore increase the polymer heterogeneity by restricting the size of continuous TPU domains. There is also a small decrease of the cooperative length of the PLLA component, but it is relatively a much smaller effect.

Despite a lowering of cooperativity length common to all multi-component samples, the glass transition temperature of the TPU intrusions is very similar to that of bulk TPU. Our calorimetry study indicates that the T_g of the nanocomposite samples with the nanotubes may be slightly lower than that of the blend without nanotubes and that of bulk TPU, but our dielectric spectroscopy data, discussed above, do

not confirm this trend. It should be remarked that the samples are stored at room temperature, that is, above the T_g of TPU, so that in order to measure this glass transition temperature the TPU component in the sample needs first be vitrified by cooling. This results in some experimental variability of the TPU T_g values. This effect, together with the relatively large uncertainty in the experimental determination of the kinetic T_g , do not allow reaching a definitive conclusion about a possible impact of the nanotubes on the glass transition temperature.

3.3. Charge conduction and interfacial polarization effects

Fig. 6(a) compares the isothermal ac conductivity spectra $\sigma''(f)$ of all studied samples at the same acquisition temperature of 373 K. The spectra of bulk TPU and of bulk, non-chain extended PLLA are also shown. The plateau-like part of all spectra at low frequency represents the dc conductivity contribution of the samples. The dc conductivity g_{PLLA} of bulk PLLA at 373 K is of the order of 10^{-14} S/cm, significantly lower than that g_{TPU} of bulk TPU, which is higher than 10^{-9} S/cm at the same temperature. As visible in the Arrhenius plot, shown in Fig. 6(b), the relation $g_{PLLA} \ll g_{TPU}$ holds in the whole probed temperature range. The Arrhenius plot of g_{TPU} exhibits a concave down curvature (non-Arrhenius behavior) which is typical of charge diffusion through disordered organic materials such as amorphous polymers [40,41]. This entails that charge conduction in pristine TPU is due to diffusion of ionic carriers, as it may be expected for a non-conjugated polymer (conjugated polymers have instead a dominant contribution from electronic charge carriers, and displays the opposite (convex, concave up) curvature in the Arrhenius plot [42] predicted by the electronic variable-range hopping model [43]).

The dc conductivity of the blends obtained with the non-reactive mixing process was very similar (within a factor of 3) to that of pristine bulk PLLA, which indicates that the long-range charge transport in the blend and nanocomposites was not strongly affected by the presence of the TPU droplets, nor by that of the CNT fillers. This can be rationalized considering that, for charge carriers to move from one electrode to the other, they must necessarily diffuse through the low-conductivity PLLA matrix, which limits the overall charge transport rate. The dc conductivity of the reactive-melt mixed blends was instead one order of magnitude higher than that of pristine PLLA, and larger by a factor of 5 that of the blends obtained by non-reactive melt mixing. This indicates that the presence of the chain-extender increases the conductivity of the PLLA matrix, possibly due to the formation of extra charge carriers (ions) in the chain-extension reactions.

We can now discuss the other relaxations visible in the high temperature dielectric spectra. Contrary to the case of the primary segmental relaxations, which displayed an asymmetric spectral profile best fitted with a Havriliak-Negami function (Eq. (1)), for the relaxation process which overlapped in frequency with the α_{PLLA} process (Fig. 3), the best fit was obtained with a Cole-Cole function, a special case of Eq. (1) with $d = 1$. The typical value of the other exponent was found to be $c \approx 0.8$. The symmetric and relatively narrow line shape of this intermediate relaxation is typically observed in phase-separated samples [44] and known as Maxwell-Wagner-Sillars (MWS) or “space-charge” relaxation. MWS relaxation processes are due to the polarization provided by

Table 2

TMDSC data for pure PLLA, pure TPU, and for the studied hybrid systems.

Sample	$T_{g,TPU}$				$T_{g,PLLA}$			
	T_g [K]	ΔC_p^{-1} [J ⁻¹ g K]	δT [K]	ξ_a [nm]	T_g [K]	ΔC_p^{-1} [J ⁻¹ g K]	δT [K]	ξ_a [nm]
Pure PLLA	–	–	–	–	332	0.363	3.5	3.4
Pure TPU	234	1.10	6	2.7	–	–	–	–
PT/CNT0/N	233	1.70	9.0	2.4	328	0.317	3.2	3.4
PT/CNT0.2/N	235	1.67	10.8	2.1	329	0.341	3.5	3.3
PT/CNT0/R	234	1.60	10.1	2.2	329	0.308	3.4	3.3
PT/CNT0.2/R	236	1.28	13.6	1.7	329	0.296	3.3	3.3

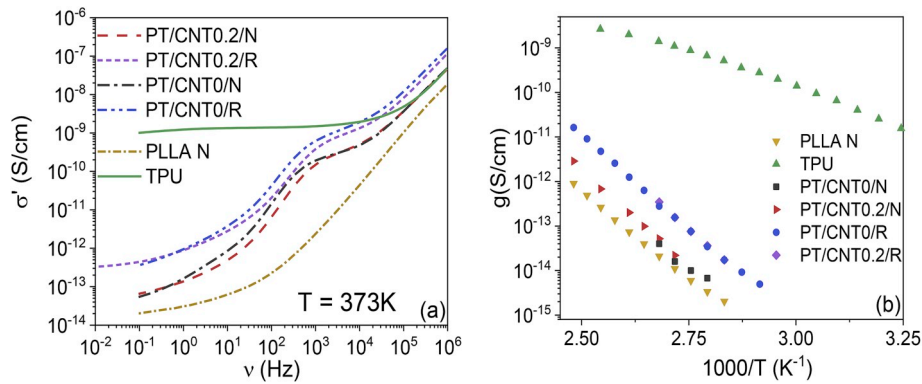


Fig. 6. (a) Ac conductivity spectra at 373 K of all studied samples. (b) Arrhenius plot of the dc conductivity of all studied samples.

charge carriers accumulated at the interface between two different phases or material domains in a heterogeneous sample [45,46].

Only one MWS process was detected in the case of the blends obtained with non-chain extended PLLA. As visible in Fig. 7(a), which reproduces part of Fig. 4, such MWS relaxation crosses the Arrhenius plot of the segmental PLLA relaxation at high temperature. On the other hand, the nanocomposites and blends prepared via reactive melt mixing were characterized by the presence of two space-charge processes, both of which cross the trace of the α_{PLLA} relaxation in the Arrhenius plot (see Fig. 7(b)).

As mentioned in the discussion of Fig. 6, the presence of the CNTs has only little influence on the ac conductivity spectra and on the plateau dc conductivity value of the blends. The small influence of the CNTs on the dc conductivity may have been anticipated given that the (macroscopic) conductivity reflects the long-range charge transport through the sample (electrode-to-electrode), whereas the nanotubes are confined in the TPU droplets and therefore contribute only marginally to the charge conduction through the PLLA matrix. By the same token, however, the presence of the CNTs in the TPU phase should result in a different, possibly increased, dc conductivity of the TPU droplets themselves. As we show in the following, this effect is indeed visible in the characteristic time of the MWS polarization at the PLLA-TPU interface.

According to the MWS theory, the space-charge relaxation frequency ω_{MW} of a sample consisting of spherical intrusions of a material with

static permittivity ϵ_p and dc conductivity g_p in a matrix of different static permittivity and conductivity ϵ_m and g_m is given by Ref. [47]:

$$\omega_{\text{MW}} = \frac{(2 + \Phi)g_m + (1 - \Phi)g_p}{(2 + \Phi)\epsilon_m + (1 - \Phi)\epsilon_p} \quad (5)$$

where Φ is the volume fraction of the dispersed phase (spherical intrusions). Since the static permittivity of an amorphous dielectric can only vary by a factor at the most of the order unity when the temperature is increased through the glass transition (due to the activation of the structural relaxation), the temperature dependence of ω_{MW} is dominated by that of the dc conductivities g_m and g_p , which in non-metallic and disordered systems has an exponential character [48]. For example, in systems where the dispersed phase has a much lower conductivity, as is the case of (nano)porous materials filled with air, the MWS relaxation has the same temperature dependence as the dc conductivity [49].

Since the weight fraction of TPU is 20 wt-% in the blends (see the experimental section), the volume fraction of the intrusions is of the order of 1/5. Taking into account moreover that $g_{\text{PLLA}} \ll g_{\text{TPU}}$, Eq. (5) can be rewritten approximately as $\omega_{\text{MW}}(T) = \frac{1}{\tau_{\text{MW}}(T)} \approx \frac{g_{\text{TPU}}(T)}{(11/4)\epsilon_{\text{PLLA}} + \epsilon_{\text{TPU}}}$. Here ϵ_{TPU} is the static permittivity of pure TPU above its glass transition temperature (at temperatures where the α_{TPU} segmental relaxation is activated), ϵ_{PLLA} is taken to be the static permittivity of PLLA below its T_g (where α_{PLLA} is not yet activated), and we have highlighted the fact that

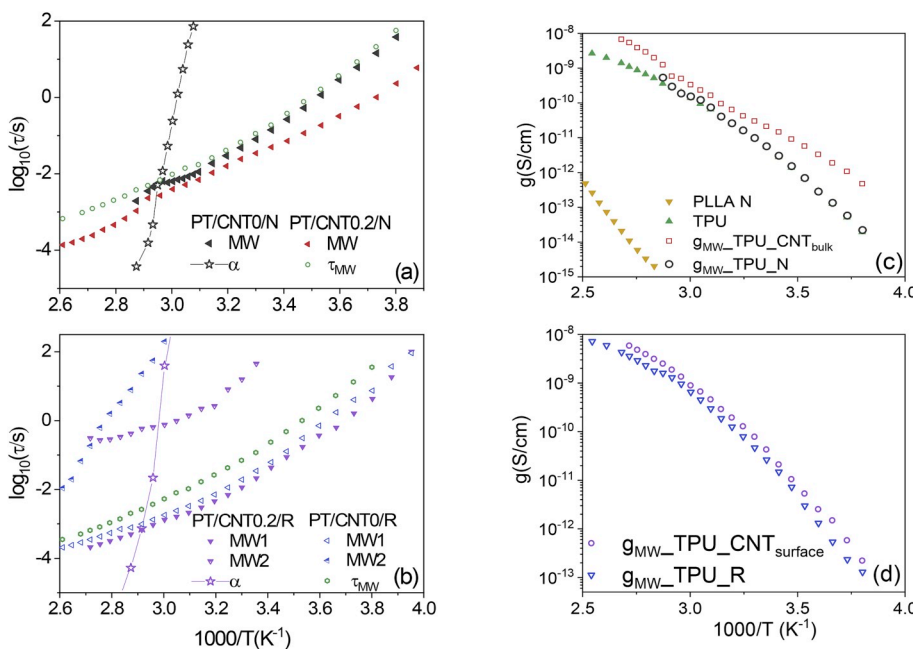


Fig. 7. (a,b) Arrhenius plot of the experimental Maxwell-Wagner-Sillars (MWS) relaxation times, and of the theoretical prediction using the reduced form of Eq. (5), for the physically melt-compounded samples (N) (panel a), and for the samples obtained by reactive mixing (R) (panel b). Two MWS processes are observed in the latter case. For completeness, also the relaxation time of the segmental α relaxation of the PLLA component is shown. (c) Arrhenius plot of the experimental dc conductivity of pure TPU and of PLLA without chain extension (empty triangles), and dc conductivity value g_{MW} calculated from the MWS relaxation times of the non-reactive melt-mixed samples. (d) Dc conductivities calculated from the shortest MWS relaxation time of the reactive-melt compounded samples.

the temperature dependence of the MWS space-charge relaxation time of our samples should follow that of the dc conductivity of the TPU component.

The MWS relaxation time predicted by the reduced version of Eq. (5) is plotted in Fig. 7(a and b). In the case of the PT/CNT0/N sample (panel (a)), the experimental MWS relaxation times coincide almost perfectly with the predicted ones. The different experimental τ_{MW} value in the PT/CNT0.2/N sample, also shown in panel (a), is caused by the presence of the nanotubes, which are dispersed in the bulk of the TPU domains (Fig. 1(a)). For both reactive-mixing (Fig. 7(b)) and non-reactive-mixing (Fig. 7(a)) samples, the MWS relaxation corresponding to the PLLA/TPU interface is observed at shorter characteristic times (larger MW frequency) in the samples containing the CNTs than in those that do not; in other words, ω_{MW} is higher in the presence of the nanotubes, irrespective of the exact location of the filler. We can therefore exploit the measured MWS relaxation times to infer an “effective” conductivity of the TPU + CNT regions by inverting the reduced form of Eq. (5), which gives:

$$g_{MW}(T) = \left(\frac{11}{4} \epsilon_{PLLA} + \epsilon_{TPU} \right) \tau_{MW} \quad (6)$$

(we employ the notation g_{MW} to signal the fact that this “effective” conductivity value is obtained from the MWS relaxation time).

Fig. 7(c) shows the Arrhenius plot of the dc conductivity of the TPU domains as extrapolated using Eq. (6) from the data of the PT/CNT0/N and PT/CNT0.2/N samples, which can be compared with the experimental conductivities of pure bulk TPU. The predicted g_{MW} of the TPU component in the blend without nanotubes (PT/CNT0/N) matches almost perfectly the experimental determination of g_{TPU} , which proves the validity of our approach. On the other hand, the TPU + CNT regions of the PT/CNT0.2/N nanocomposite blend have higher conductivity, on average by a factor of 10, due to the beneficial effect of the carbon nanotube fillers. The same effect is also visible, although by a smaller factor, in the case of the PT/CNT0/R and PT/CNT0.2/R blends (Fig. 7(d)). Our nanocomposite blends display therefore a selective conductivity enhancement of only the TPU nanodomains.

Comparison with theory for the reactive melt-mixing samples is not carried out, because the temperature-dependent dc conductivity of homogeneous amorphous chain-extended PLLA could not be measured due to its strong tendency to crystallize just above T_g [2], and to the non-homogeneous dispersion of the CNT filler, which is present at the interface between the two polymers (Fig. 1(b)) rather than in the bulk of the TPU phase. The lower impact of the carbon nanotubes in reactive melt-compounded samples is nonetheless ascribable both to a lower impact of the filler on the conductivity of the TPU phase, and to the higher conductivity of the chain-extended PLLA compared to pristine PLLA.

Despite the fact that the weight fraction of functionalized CNTs in the TPU phase (1%) is close to the percolation threshold reported for the carboxylated CNT-TPU nanocomposite [31], the phase-selective conductivity enhancement is relatively low (only one order of magnitude). It is also worth pointing out that the Arrhenius plot of the dc conductivity of the TPU droplets, as inferred from the MWS relaxation, displays a curvature which might be consistent with diffusional charge transport of ionic, rather than electronic, charge carriers. Since the MWS arises from an interfacial polarization effect at the TPU-PLLA separation, and since the conductivity of the pristine TPU matrix is ionic in nature, it could be that the dielectric interfacial relaxation time reflects an increased ionic conductivity of the TPU phase, rather than the contribution of the diffusion electronic charge carriers along the nanotube network. An increase of the ionic conductivity has been reported in other nanocomposites consisting of distinct polymer-filler pairs, including also systems with CNTs [50,51]. Whichever the case, our results show that dielectric spectroscopy provides a means to distinguish, in a bulk nanocomposite, between the long-range overall conductivity and the conductivity of the dispersed phase.

Interestingly, the reactive melt-compounded samples exhibited two MWS processes, whose relaxation times are displayed in Fig. 7(b) together with the predicted values using the reduced form of Eq. (5). The faster MWS process in these samples coincides with that of the non-reactive melt-compounded ones, which is the one we have discussed so far. As for the slower MWS process, the fact that it is observed also in reactive-melt mixed blends without nanotubes indicates that it is not strictly due to the presence of the CNT fillers. We recently reported a low-frequency space-charge process in chain extended PLLA and nanocomposites of PLLA with carboxylated CNTs [2], which we tentatively assigned to the charge accumulation at heterogeneities induced by the presence of the chain-extender molecules. We therefore assign the slower MWS process in the reactive melt-compounded samples to the same type of heterogeneities produced by the chain extension reaction. The fact that this slower MW process occurs at lower frequency (i.e., longer times) is consistent with the lower conductivity of the PLLA matrix compared with that of TPU, since a MWS relaxation within the bulk PLLA phase should have a characteristic angular frequency of the order of $\omega_{MW,PLLA} = \frac{g_{PLLA}}{\epsilon_{PLLA}}$. The significant difference of this PLLA-related MWS relaxation time in the presence of the CNT filler is likely due to the interaction between the chain-extended PLLA with the functional CNTs, which is also responsible for the presence of the filler at the surface of the TPU intrusions (Fig. 1(b)).

3.4. Secondary relaxations

We finally analyze the secondary relaxations detected in our samples. As visible in Fig. 4, the nanocomposite blends displayed two “fast” relaxations, whose characteristic times matched very roughly the temperature dependence of the secondary (local) relaxation dynamics of the pure PLLA and TPU polymers. Of the two, the relaxation time of the fastest relaxation of the nanocomposite blends matched roughly that of the γ relaxation of pristine TPU, which is associated with the crankshaft motion of $(CH_2)_n$ sequences that involves the reorientation of oxygen-containing polar groups covalently linked to them [34]. While the dielectric strength of the γ relaxation is relatively high in pristine TPU (even comparable to the structural relaxation), in the nanocomposite blends it has a much lower intensity due to the relatively low volume fraction of TPU in the sample. In the nanocomposite blend obtained by non-reactive melt-compounding, in which the CNT fillers are dispersed in the volume of the TPU intrusions, this relaxation is altogether missing, which perhaps indicates that the H-bond interactions between the polar groups of the TPU chains and the rigid functionalized CNT partially suppress the crankshaft dynamics of the $(CH_2)_n$ backbone.

The secondary relaxation with longer characteristic time of the nanocomposites is observed in the expected spectral range of both the secondary β relaxation of pure PLLA, which is due to small-angle twisting motions of the main chain [52], and the β relaxation of pure TPU, associated with reorientational motions of the ester complexes [34] and strongly influenced by the presence of water impurities [53]. This β relaxation displayed a significant change in the presence of the CNT fillers, which is visible in both types of samples. Unfortunately, we are not able to give a precise assignment of this secondary relaxation, since the local relaxations of both polymers may contribute to the indicated spectral feature, and moreover the TPU β relaxation is sensitive to the water content in the sample, on which we do not have control.

4. Conclusions

Nanocomposites consisting of carboxylated carbon nanotubes (CNTs) dispersed in a binary polylactic acid (PLLA) – thermoplastic polyurethane (TPU) blend have been studied in this work. The nanocomposite blends were obtained both by nonreactive and reactive mixing (with a PLLA chain extender) in the molten state. The binary PLLA/TPU blend was characterized by phase separation into TPU

droplets of submicron size dispersed in the PLLA matrix, with two separate glass transition temperatures. Despite being initially dispersed in the PLLA matrix, in the nanocomposite blends the carbon nanotubes were present either in the TPU droplets (in the case of samples obtained without chain extender), or at their boundaries (in the case of reactive-melt mixed samples). The samples produced by non-reactive and reactive melt-mixing displayed respectively five and six distinct dielectric relaxations, which we were able to assign to different dielectric phenomena. The TPU submicron confinement in droplets lead to a decrease of the cooperativity length of the segmental relaxation of the TPU phase, which is accentuated by the presence of the CNT fillers. The nanofiller is also found to speed up the local secondary relaxation of the TPU polymer.

Samples obtained by non-reactive melt mixing displayed a single space-charge relaxation associated to the PLLA/TPU interface, while the reactive melt mixed ones displayed two. One of the observed space-charge relaxations stems from the heteropolymer interface, while the other is due to intra-PLLA heterogeneities induced by the presence of the chain extensions. Ac conductivity measurements show that the CNTs do not contribute directly to the long-range charge transport in the nanocomposite blends, as expected from their localized character. Instead, we observed an increase in the frequency of the Maxwell-Wagner-Sillars space-charge relaxation due to charge accumulation at the PLLA-TPU boundary. According to Eq. (6), this is due to the increased conductivity of either the TPU intrusions or of the TPU/PLLA interface due to the presence of the CNT fillers result. Our results demonstrate a selective conductivity enhancement of the polyurethane component due to the presence of the fillers, both when they lay in the volume of the TPU intrusions or at their surface. The resulting interfacial dielectric effect might be due to the increase of the ionic, rather than electronic, charge transport.

Declaration of competing interest

The authors declare that they have no known competing financial interests or personal relationships that could have appeared to influence the work reported in this paper.

CRediT authorship contribution statement

Sofia Valenti: Investigation, Validation, Visualization, Writing - original draft. **Omid Yousefzade:** Validation, Investigation, Visualization. **Jordi Puiggalí:** Funding acquisition, Project administration, Resources. **Roberto Macovez:** Conceptualization, Supervision, Funding acquisition, Writing - review & editing.

Acknowledgements

J.P., R.M. and S.V. are grateful to acknowledge support from the Spanish Ministry of Economy and Competitiveness MINECO and FEDER (projects MAT2015-69547-R and FIS2017-82625-P). R.M. and J.P. acknowledge support by the Generalitat de Catalunya under projects 2017SGR-42 and 2017SGR-373, respectively.

References

- [1] S. Thomas, D. Rouxel, D. Ponnammam (Eds.), *Spectroscopy of Polymer Nanocomposites*, Elsevier, 2016.
- [2] O. Yousefzade, S. Valenti, J. Puiggalí, H. Garmabi, R. Macovez, Segmental relaxation and partial crystallization of chain-extended Poly(L-lactic acid) reinforced with carboxylated carbon nanotube, *J. Polym. Sci. B Polym. Phys.* 57 (2019) 222–233, <https://doi.org/10.1002/polb.24774>.
- [3] I. Khan, M. Mansha, M.A. Jafar Mazumder, Chapter 16: polymer blends, in: *Functional Polymers, Polymers and Polymeric Composites: A Reference Series*, Springer, Cham, 2018.
- [4] S. Fu, Z. Sun, P. Huang, Y. Li, N. Hu, Some basic aspects of polymer nanocomposites: a critical review, *Nano Mat. Sci.* 1 (2019) 2–30, <https://doi.org/10.1016/j.nanoms.2019.02.006>.
- [5] R.J. Young, I.A. Kinloch, L. Gong, K.S. Novoselov, The mechanics of graphene nanocomposites: a review, *Compos. Sci. Technol.* 72 (2012) 1459–1476, <https://doi.org/10.1016/j.compscitech.2012.05.005>.
- [6] W. Bauhofer, J.Z. Kovacs, A review and analysis of electrical percolation in carbon nanotube polymer composites, *Compos. Sci. Technol.* 69 (2009) 1486–1498, <https://doi.org/10.1016/j.compscitech.2008.06.018>.
- [7] E.I. Akpan, X. Shen, B. Wetzel, K. Friedrich, Design and synthesis of polymer nanocomposites, in: *Polymer Composites with Functionalized Nanoparticles*, Elsevier, 2019, pp. 47–83.
- [8] L. Zhang, T.J. Webster, Nanotechnology and nanomaterials: promises for improved tissue regeneration, *Nano Today* 4 (2009) 66–80, <https://doi.org/10.1016/j.nantod.2008.10.014>.
- [9] N. Karak, Fundamentals of nanomaterials and polymer nanocomposites, in: *Nanomaterials and Polymer Nanocomposites*, Elsevier, 2019, pp. 1–45.
- [10] L.T. Lim, R. Auras, M. Rubino, Processing technologies for poly(lactic acid), *Prog. Polym. Sci.* 33 (2008) 820–852, <https://doi.org/10.1016/j.progpolymsci.2008.05.004>.
- [11] G. Perego, G.D. Cella, C. Bastioli, Effect of molecular weight and crystallinity on poly(lactic acid) mechanical properties, *J. Appl. Polym. Sci.* 59 (1996) 37–43, <https://doi.org/10.1016/j.progpolymsci.2008.05.004>.
- [12] N. Najafi, M.C. Heuzey, P.J. Carreau, Poly(lactide) (PLA)-clay nanocomposites prepared by melt compounding in the presence of a chain extender, *Compos. Sci. Technol.* 72 (2012) 608–615, <https://doi.org/10.1016/j.compscitech.2012.01.005>.
- [13] V. Arias, K. Odellius, A. Höglund, A.-C. Albertsson, Homocomposites of polylactide (PLA) with induced interfacial stereocomplex crystallites, *ACS Sustain. Chem. Eng.* 3 (2015) 2220–2231, <https://doi.org/10.1021/acssuschemeng.5b00498>.
- [14] S.-Y. Zhou, H.-D. Huang, X. Ji, D.-X. Yan, G.-J. Zhong, B.S. Hsiao, Z.-M. Li, Superrobust polylactide barrier films by building densely oriented lamellae incorporated with ductile in situ nanofibrils of poly(butylene adipate-co-terephthalate), *ACS Appl. Mater. Interfaces* 8 (2016) 8096–8109, <https://doi.org/10.1021/acsami.6b00451>.
- [15] F. Yu, H.-X. Huang, Simultaneously toughening and reinforcing poly(lactic acid)/thermoplastic polyurethane blend via enhancing interfacial adhesion by hydrophobic silica nanoparticles, *Polym. Test.* 45 (2015) 107–113, <https://doi.org/10.1016/j.polymertesting.2015.06.001>.
- [16] M. Raja, S.H. Ryu, A.M. Shanmugharaj, Thermal, mechanical and electroactive shape memory properties of polyurethane (PU)/poly(lactic acid) (PLA)/CNT nanocomposites, *Eur. Polym. J.* 49 (2013) 3492–3500, <https://doi.org/10.1016/j.eurpolymj.2013.08.009>.
- [17] V. Jašo, M. Cvetinov, S. Rakić, Z.S. Petrović, Bio-plastics and elastomers from polylactic acid/thermoplastic polyurethane blends, *J. Appl. Polym. Sci.* 131 (2014) 41104, <https://doi.org/10.1002/app.41104>.
- [18] S.-M. Lai, Y.-C. Lan, Shape memory properties of melt-blended polylactic acid (PLA)/thermoplastic polyurethane (TPU) bio-based blends, *J. Polym. Res.* 20 (2013) 140, <https://doi.org/10.1007/s10965-013-0140-6>.
- [19] X. Lu, X. Wei, J. Huang, L. Yang, G. Zhang, G. He, M. Wang, J. Qu Supertoughened, Poly(lactic acid)/polyurethane blend material by in situ reactive interfacial compatibilization via dynamic vulcanization, *Ind. Eng. Chem. Res.* 53 (2014) 17386–17393, <https://doi.org/10.1021/ie503092w>.
- [20] O. Yousefzade, H. Garmabi, J. Puiggalí, M. Heydarnejad Moghadam, Rigid amorphous phase and constrained polymer chains in poly(L-lactide) nanocomposites with carboxylated carbon nanotubes prepared via reactive melt mixing, *Polym. Compos.* 39 (2018) E1280–E1293, <https://doi.org/10.1002/pc.24856>.
- [21] S. Havriliak, S. Negami, A complex plane analysis of α -dispersions in some polymer systems, *J. Polym. Sci., Polym. Chem. Ed.* 16 (1966) 99–117, <https://doi.org/10.1002/polc.5070140111>.
- [22] S. Havriliak, S. Negami, A complex plane representation of dielectric and mechanical relaxation processes in some polymers, *Polymer* 8 (1967) 161–210, [https://doi.org/10.1016/0032-3861\(67\)90021-3](https://doi.org/10.1016/0032-3861(67)90021-3).
- [23] K.S. Cole, R.H. Cole, Dispersion and absorption in dielectrics - I alternating current characteristics, *J. Chem. Phys.* 9 (1941) 341–352, <https://doi.org/10.1063/1.1750906>.
- [24] K.S. Cole, R.H. Cole, Dispersion and absorption in dielectrics - II direct current characteristics, *J. Chem. Phys.* 10 (1942) 98–105, <https://doi.org/10.1063/1.1723677>.
- [25] O. Yousefzade, J.M. Ugartemendia, L. Sangroniz, R. Hernandez, J. Puiggalí, H. Garmabi, Selective localization of carboxylated carbon nanotubes in blends of poly(L-lactide) and thermoplastic polyurethane prepared via reactive melt mixing, *J. Mater. Sci.* 54 (2019) 14961–14974, <https://doi.org/10.1007/s10853-019-03889-8>.
- [26] M.R. Aghjeh, V. Asadi, P. Mehdijabbar, H.A. Khonakdar, S.H. Jafari, Application of linear rheology in determination of nanoclay localization in PLA/EVA/Clay nanocomposites: correlation with microstructure and thermal properties, *Compos. B Eng.* 86 (2016) 273–284, <https://doi.org/10.1016/j.compositesb.2015.09.064>.
- [27] A.H.A. Hoseini, M. Arjmand, U. Sundararaj, M. Trifkovic, Tunable electrical conductivity of polystyrene/polyamide-6/carbon nanotube blend nanocomposites via control of morphology and nanofiller localization, *Eur. Polym. J.* 95 (2017) 418–429, <https://doi.org/10.1016/j.eurpolymj.2017.08.037>.
- [28] E. Jalali Dil, B.D. Favis, Localization of micro- and nano-silica particles in heterophase poly(lactic acid)/poly(butylene adipate-co-terephthalate) blends, *Polymer* 76 (2015) 295–306, <https://doi.org/10.1016/j.polymer.2015.08.046>.
- [29] C. Laurent, E. Flahaut, A. Peigney, The weight and density of carbon nanotubes versus the number of walls and diameter, *Carbon* 48 (2010) 2994–2996, <https://doi.org/10.1016/j.carbon.2010.04.010>.

- [30] N. Chiodarelli, O. Richard, H. Bender, M. Heyns, S. De Gendt, G. Groeseneken, P. M. Vereecken, Correlation between number of walls and diameter in multiwall carbon nanotubes grown by chemical vapor deposition, *Carbon* 50 (2012) 1748–1752, <https://doi.org/10.1016/j.carbon.2011.12.020>.
- [31] K. Wongtimnoi, B. Guiffard, A. Bogner-Van de Moortèle, L. Seveyrat, J.-Y. Cavaillé, Electrostrictive thermoplastic polyurethane-based nanocomposites filled with carboxyl-functionalized multi-walled carbon nanotubes (MWCNT-COOH): properties and improvement of electromechanical activity, *Compos. Sci. Technol.* 85 (2013) 23–28, <https://doi.org/10.1016/j.compscitech.2013.05.015>.
- [32] S. Valenti, A. Diaz, M. Romanini, L.J. del Valle, J. Puiggali, J. Li Tamarit, R. Macovez, Amorphous binary dispersions of chloramphenicol in enantiomeric pure and racemic poly-lactic acid: morphology, molecular relaxations, and controlled drug release, *Int. J. Pharm.* 568 (2019) 118565, <https://doi.org/10.1016/j.ijpharm.2019.118565>.
- [33] S. Valenti, M. Romanini, L. Franco, J. Puiggali, J. Li Tamarit, R. Macovez, Tuning the kinetic stability of the amorphous phase of the chloramphenicol antibiotic, *Mol. Pharm.* 15 (2018) 5615–5624, <https://doi.org/10.1021/acs.molpharmaceut.8b00786>.
- [34] G. Polizos, E. Tuncer, A.L. Agapov, D. Stevens, A.P. Sokolov, M.K. Kidder, J. D. Jacobs, H. Koerner, R.A. Vaia, K.L. More, I. Sauer, Effect of polymer-nanoparticle interactions on the glass transition dynamics and the conductivity mechanism in polyurethane titanium dioxide nanocomposites, *Polymer* 53 (2012) 595–603, <https://doi.org/10.1016/j.polymer.2011.11.050>.
- [35] C.A. Angell, Structural instability and relaxation in liquid and glassy phases near the fragile liquid limit, *J. Non-Cryst. Solids* 102 (1988) 205–221, [https://doi.org/10.1016/0022-3093\(88\)90133-0](https://doi.org/10.1016/0022-3093(88)90133-0).
- [36] G. Adam, J.H. Gibbs, On the temperature dependence of cooperative relaxation properties in glass-forming liquids, *J. Chem. Phys.* 43 (1965) 139–146, <https://doi.org/10.1063/1.1696442>.
- [37] E. Donth, The size of cooperatively rearranging regions at the glass transition, *J. Non-Cryst. Solids* 53 (1982) 325–330, [https://doi.org/10.1016/0022-3093\(82\)90089-8](https://doi.org/10.1016/0022-3093(82)90089-8).
- [38] E. Donth, Characteristic length of the glass transition, *J. Polym. Sci. B Polym. Phys.* 34 (1996) 2881–2892, [https://doi.org/10.1002/\(SICI\)1099-0488\(199612\)34:17<2881::AID-POLB3>3.0.CO;2-U](https://doi.org/10.1002/(SICI)1099-0488(199612)34:17<2881::AID-POLB3>3.0.CO;2-U).
- [39] E. Hempel, G. Hempel, A. Hensel, C. Schick, E. Donth, Characteristic length of dynamic glass transition near T_g for a wide assortment of glass-forming substances, *J. Phys. Chem. B* 104 (2000) 2460–2466, <https://doi.org/10.1021/jp991153f>.
- [40] C. Do, P. Lunkenheimer, D. Diddens, M. Götz, M. Weiß, A. Loidl, X.-G. Sun, J. Allgaier, M. Ohl, Li^+ transport in poly(ethylene oxide) based electrolytes: neutron scattering, dielectric spectroscopy, and molecular dynamics simulations, *Phys. Rev. Lett.* 111 (2013), 018301, <https://doi.org/10.1103/PhysRevLett.111.018301>.
- [41] M. Zachariah, M. Romanini, P. Tripathi, J. Li Tamarit, R. Macovez, Molecular diffusion and dc conductivity perfectly correlated with molecular rotational dynamics in a plastic crystalline electrolyte, *Phys. Chem. Chem. Phys.* 17 (2015) 16053–16057, <https://doi.org/10.1039/C5CP02345A>.
- [42] S. Capaccioli, M. Lucchesi, P.A. Rolla, G. Ruggeri, Dielectric response analysis of a conducting polymer dominated by the hopping charge transport, *J. Phys. Condens. Matter* 10 (1998) 5595–5617, <https://doi.org/10.1088/0953-8984/10/25/011>.
- [43] R. Macovez, M. Zachariah, M. Romanini, P. Zygori, D. Gournis, J. Li Tamarit, Hopping conductivity and polarization effects in a fullerene derivative salt, *J. Phys. Chem. C* 118 (2014) 12170–12175, <https://doi.org/10.1021/jp503298e>.
- [44] M. Zachariah, M. Romanini, P. Tripathi, M. Barrio, J. Li Tamarit, R. Macovez, Self-diffusion, phase behavior, and Li^+ ion conduction in succinonitrile-based plastic Co-crystals, *J. Phys. Chem. C* 119 (2015) 27298–27306, <https://doi.org/10.1021/acs.jpcc.5b09380>.
- [45] J.C. Maxwell, *Electr. Magn.* 1 (1892) 452. London.
- [46] K.W. Wagner, Erklärung der dielektrischen Nachwirkungsvorgänge auf Grund Maxwellscher Vorstellungen, *Arch. Electrotech.* 2 (1914) 371, <https://doi.org/10.1007/BF01657322>.
- [47] T. Hanai, Dielectric theory on the interfacial polarization for two-phase mixtures, *Bull. Inst. Chem. Res. Kyoto Univ.* 39 (1962) 341–367.
- [48] J.C. Dyre, T.B. Schroder, Universality of Ac conduction in disordered solids, *Rev. Mod. Phys.* 72 (2000) 873–892, <https://doi.org/10.1103/RevModPhys.72.873>.
- [49] G.N. Ruiz, I. Combarro-Palacios, S.E. McLain, G.A. Schwartz, L.C. Pardo, S. Cervený, R. Macovez, Tuning molecular dynamics by hydration and confinement: antiplasticizing effect of water in hydrated prilocaine nanoclusters, *Phys. Chem. Chem. Phys.* 21 (2019) 15576, <https://doi.org/10.1039/C9CP01771B>.
- [50] G.B. Appetecchi, F. Croce, G. Dautzenberg, M. Mastragostino, F. Ronci, B. Scrosati, F. Soavi, A. Zanelli, F. Alessandrini, P.P. Prosini, Composite polymer electrolytes with improved lithium metal electrode inter-facial properties. I. Electrochemical properties of dry PEO-LiX systems, *J. Electrochem. Soc.* 145 (1998) 4126–4132, <https://doi.org/10.1149/1.1838925>.
- [51] C. Tang, K. Hackenberg, Q. Fu, P.M. Ajayan, H. Ardebili, High ion conducting polymer nanocomposite electrolytes using hybrid nanofillers, *Nano Lett.* 12 (2012) 1152–1156, <https://doi.org/10.1021/nl202692y>.
- [52] J. Ren, K. Adachi, Dielectric relaxation in blends of amorphous poly(DL-lactic acid) and semicrystalline poly(L-lactic acid), *Macromolecules* 36 (2003) 5180–5186, <https://doi.org/10.1021/ma034420v>.
- [53] G. Polizos, E. Tuncer, V. Tomer, I. Sauer, C.A. Randall, E. Manias, Dielectric spectroscopy of polymer-based nanocomposite dielectrics with tailored interfaces and structured spatial distribution of fillers, in: S.M. Musa (Ed.), *Nanoscale Spectroscopy with Applications*, CRC Press, 2013.